

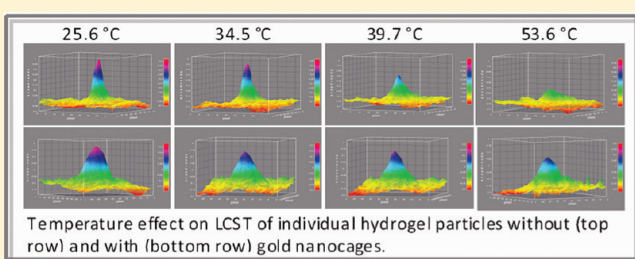
Visualizing the Effect of Gold Nanocages on Absorption, Imaging, and Lower Critical Solution Temperature Phase Transition of Individual Poly(NiPAM)-Based Hydrogel Particles by Near Infrared Multispectral Imaging Microscopy

Irena Mejac and Chieu D. Tran*

Department of Chemistry, Marquette University, P.O. Box 1881, Milwaukee, Wisconsin 53201, United States

 Supporting Information

ABSTRACT: We have successfully utilized the near-infrared multispectral imaging (NIR-MSI) microscope to observe and measure directly images and spectra of individual hydrogel particles alone or with added gold nanocages (GNs). The NIR-MSI is suited for this task because it can simultaneously record spectral and spatial information of a sample with high sensitivity (single pixel resolution) and high spatial resolution ($\sim 0.9 \mu\text{m}/\text{pixel}$). Because both images and spectra of the individual particles can be directly and simultaneously measured by the microscope, it is possible to detect any changes in the spectroscopic properties and/or nature (size, volume) of individual hydrogel particles induced by external factors (e.g., temperature and/or pH). These features make it possible to determine lower critical solution temperature (LCST) values based on monitoring either changes in the NIR spectra or the volume of the hydrogel particle in response to variations in temperature. More importantly, the measured volume transition temperature or LCST value is not of a collection of many hydrogel particles, but rather of individual hydrogel particles. GNs were found to significantly affect not only absorption but also images and properties of individual hydrogel particles. Specifically, GNs were found to enhance absorption of individual hydrogel particles, particularly the C–H band at 1716 nm, by about 25%. Of particular interest is the fact that not all individual hydrogel particles were enhanced by GNs; only about 50% of total number of particles were enhanced by GNs. GNs were also found to make it difficult to observe individual hydrogel particles, i.e., it seems that GNs defocused images of hydrogel particles. The defocusing effect by GNs might be due to photothermal generation of heat and vapor bubbles by the GNs. Of particular interest is the effect of GNs on the volume transition temperature of individual hydrogel particles. It seems that individual hydrogel particles lose their LCST in the presence of GNs, i.e., when heated, they undergo a gradual decrease in the volume but do not exhibit any clear and observable discontinued phase transition temperature.



Noble metal nanoparticles exhibit a strong absorption band that is not present in the spectrum of the bulk metal. This absorption band arises when the incident photon frequency is resonant with the collective oscillation of the electrons and is known as the localized surface plasmon resonance (LSPR).^{1–3} The LSPR enables noble metal nanoparticles to provide substantial enhancement for a variety of spectroscopic processes including surface-enhanced Raman spectroscopy (SERS). The properties of the LSPR are known to be dependent on the dielectric function of the constituent metal and the embedding medium, and also on the size, shape, and morphology of the nanostructure.^{1–3} Considerable efforts have been made in the past few years to prepare different types of noble metal nanoparticles whose LSPR can be controlled and adjusted for appropriate applications and devices. Of particular interest are gold nanocages.^{4–7} Gold nanocages (GNs) are hollow, gold–silver alloyed nanostructures synthesized through a straightforward galvanic replacement reaction between a silver nanoparticle and a gold precursor (chloroauric acid).^{4–6} The LSPR properties of GNs can be easily tuned across the visible spectrum and into the NIR range, making them an ideal

candidate to enhance absorption and optical signals for a wide variety of imaging and therapeutic techniques.^{4–6} It would, therefore, be interesting to determine if nanocages can enhance absorption of a polymer molecule with sizes larger than 1 μm , and if enhanced absorption will have any effect on image of the polymer molecules recorded in the region of the polymer absorption.

Water-soluble hydrogel polymers such as poly(*n*-isopropylacrylamide) (poly(NIPAM)) have drawn the interest of scientists and engineers due to their unique responsive behavior to external stimuli (e.g., temperature and pH).⁷ For example, samples of poly(NIPAM) in aqueous solution are known to rapidly undergo volume transitions at the lower critical solution temperature (LCST), namely, poly(NIPAM) microstructures in aqueous solution are hydrophilic and swollen below the LCST but become hydrophobic and collapsed above the LCST.^{8–10}

Received: January 27, 2011

Accepted: March 18, 2011

Published: April 08, 2011

Importantly, poly(NIPAM) and particularly its copolymer with acrylic acid, poly(NIPAM-co-AAc), exhibit LCST transitions near physiologic temperature, which has motivated research efforts directed toward various biomedical applications, including those involving drug delivery.^{6,7,11,12} Efforts have been made in the past few years, using a variety of techniques including calorimetry, NMR, fluorescence, dynamic light scattering, neutron scattering, and dielectric relaxation, to determine onset temperatures and mechanism of LCST of poly(NIPAM) in water.^{14–20} Limited success has been achieved because these studies are plagued by variations in size, morphology, and stability of poly(NIPAM). Specifically, the polydispersity of hydrogel particles leads to strong inhomogeneities in their spectroscopic response and hinders the comparison of data obtained from independent experiments and also data obtained from experiment and computation. As a consequence, a technique that is capable of measuring the spectroscopic properties of single hydrogel particles is particularly needed.

It is of particular interest to determine if GNs can be used to enhance absorption and visualization of individual polymer particles as large as hydrogel particles (i.e., larger than 1 μm) so that response not of a collection of many hydrogel particles but rather of individual particles to external stimulus such as temperature can be monitored. Such a study will also need a technique which can simultaneously measure absorption spectra and images with spatial resolution less than 1 μm so that individual hydrogel particles can be observed, measured, and monitored as they interact with GNs and undergo phase transition temperature. The near-infrared multispectral imaging (NIR-MSI) microscope based on an acousto-optic tunable filter (AOTF), which was developed in our group, with its unique features is particularly suited for this task.^{21–26}

A multispectral imaging spectrometer is an instrument that can simultaneously record spectral and spatial information about a sample.^{21,27} Unlike conventional imaging techniques, which rely on recording a single image using either single or multi-wavelength light for illumination, the multispectral imaging technique records a series of several thousand images, each image at a specific wavelength. That is, it measures absorption spectra of a sample not at a single position, as is the case for a conventional spectrophotometer, but simultaneously at many different positions within a sample (by using a focal plane array detector rather than a single channel detector).^{21,27} Chemical composition and structure at different positions within a sample can be elucidated from such images.¹¹ We have recently developed a near-infrared (NIR) multispectral imaging microscope that employs an acousto-optic tunable filter (AOTF) for rapid spectral tuning and a microscope for higher spatial resolution.^{21–26} The high sensitivity, fast temporal (milliseconds), and high spatial resolution ($\sim\mu\text{m}$) of this imaging microscope make it possible for us to use this multispectral imaging microscope for studies and measurements that, to date, have not been possible using existing techniques. These include photoinduced changes of a single unit micrometer-size cell in temperature-sensitive liquid crystals as a function of time and wavelength,^{21–26} and the determination of molecular state and distribution of fullerenes entrapped in sol–gel samples.²⁵

The information presented in the present manuscript is indeed provocative and clearly indicates that it may be possible for GNs to enhance absorption and to facilitate observation and monitoring of individual polymer particles as large as hydrogel particles (i.e., larger than 1 μm). Such consideration prompted us to initiate this study which aims to explore the use of GNs to

enhance absorption of hydrogel particles and to use the NIR-MSI microscope to observe, measure, and monitor response, not of a collective but rather of individual hydrogel particles. The results of our initial investigation are reported herein.

■ EXPERIMENTAL SECTION

Detailed information on the synthesis and characterization of poly-N-isopropylacrylamide-acrylic acid (PNiPAM-AAc) hydrogel particles^{28,29} together with instrumentation and performance characteristics of the AOTF-based NIR-MSI microscope can be found in the Supporting Information. Gold nanocages were obtained from Claire Cobley of Prof. Younan Xia's group at Department of Biomedical Engineering, Washington University, St. Louis, MO. They were synthesized with previously reported procedures.^{30,31} These nanocages were composed of a gold–silver alloy with an edge length of ~ 150 nm, and a localized surface plasmon resonance (LSPR) spectrum of these nanocages which exhibits $\lambda_{\max} \sim 1304$ nm is shown in Figure S1 of Supporting Information.

■ RESULTS AND DISCUSSION

The spatial resolution of the NIR-MSI microscope is $0.93 \pm 0.03 \mu\text{m}/\text{pixel}$ (see detailed description in Supporting Information). Since the average diameter of the hydrogel particle used in this study is $\geq 1.0 \mu\text{m}$, the individual hydrogel can be observed and measured by the multispectral imaging microscope. The two dimensional (2-D) image (recorded at 1764 nm) of the hydrogel particle is shown in the top of Set A in Figure 1 (where the hydrogel particle is dark blue, the background is green, and the black line is the NIR camera marking) (Images at 1764 nm instead of at λ_{\max} of the band at 1716 nm are shown because the contrast ratio is optimal at this wavelength). A selected section of the 2-D images was taken to calculate a corresponding 3-D plot of the absorbance of a single hydrogel particle at 1764 nm, and the image obtained is shown in the bottom of Set A of Figure 1 where the units of x , y , and z axis are pixel, pixel, and absorbance, respectively. Dimensions of the hydrogel particle, calculated from the image (based on the relationship $0.93 \pm 0.03 \mu\text{m}/\text{pixel}$), was found to be $3.1 \pm 0.4 \mu\text{m}$.

To further characterize the hydrogel particles, NIR absorption spectra of eight different single individual poly NiPAM-AAc hydrogels were calculated from recorded images from 1580 to 2200 nm, and the spectra obtained are shown in Figure S2A of Supporting Information. It is noteworthy to add that each of these spectra was calculated from recorded images using data from a single pixel. It is pleasing to see that the S/N of the imaging instrument is very good even at single pixel scale. The fact that these spectra are very similar even though they were obtained from various single hydrogel particles with various sizes (from as small as 1.4 μm to as large as 3.19 μm) clearly indicates that there is no observable chemical heterogeneity among these hydrogel particles. The averaged NIR spectrum of these eight single particles together with associated standard deviations is shown in Figure S2B of Supporting Information. As illustrated, the relative difference among NIR spectra of single particles is relatively small; the largest relative error was found to be 3.8%. As can be seen from the spectra, in this NIR region, the hydrogel particles exhibit two strong absorption bands at around 1716 and 2010 nm. The former band can be attributed to the C–H overtone and combination transition while the latter is due to the overtone of the O–D transition of D₂O and of the carboxylic acid group of the hydrogels (through deuterium exchange with D₂O).

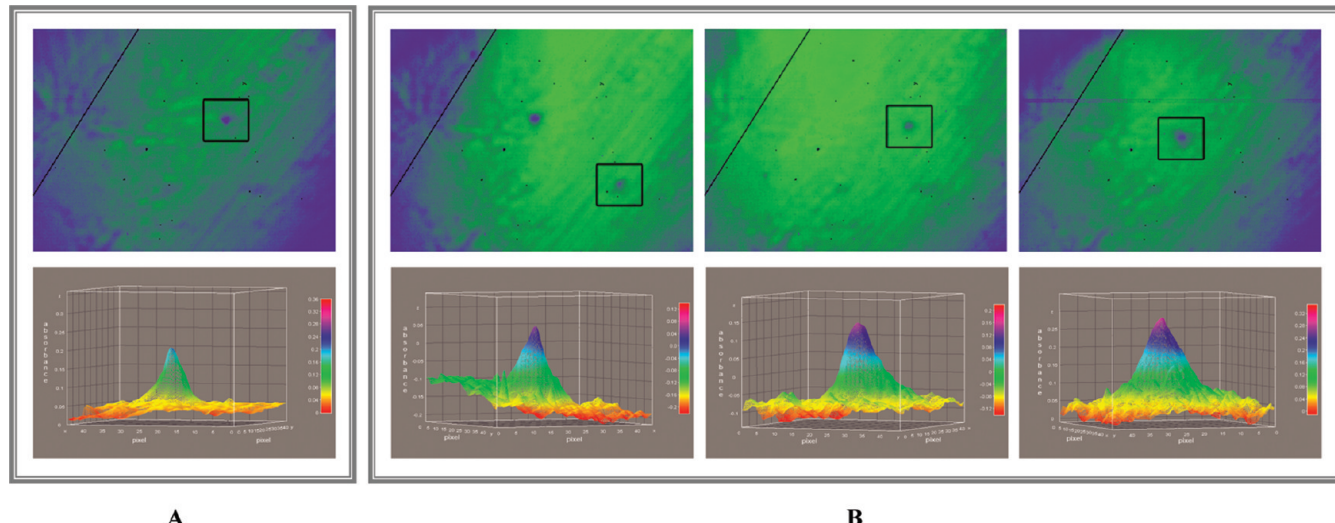


Figure 1. 2-D images (top) and corresponding 3-D images (bottom) of the drawn rectangular section in 2-D images of absorption at 1764 nm of hydrogel particles without gold nanocages (Set A) and with gold nanocages (Set B). Units for x , y , and z axes are pixel, pixel, and absorbance at 1764 nm, respectively (one pixel corresponds to $0.93 \mu\text{m}$).

As described in the previous section, relative scattering intensity and absorption cross-sections of gold nanocages (GNs) are known to be dependent on their size whereas their LSPR band position can be tuned throughout the visible and into the NIR region by adjusting conditions of the galvanic replacement reaction.^{4–6} Synthesis of the GNs used in this study was designed and selected to provide nanocages with large LSPR in the NIR region. As expected, the absorption spectrum of the GNs in D_2O taken on an NIR spectrophotometer, shown in Figure S1 of Supporting Information, exhibits a broad and pronounced LSPR band with $\lambda_{\text{max}} \sim 1304 \text{ nm}$. Since the LSPR band of the GNs is in the same spectral region as the absorption band of the hydrogels, it is anticipated that the GNs can enhance absorption of the hydrogels. This possibility is investigated, and results are shown in following section.

Set B of Figure 1 shows 2-D and corresponding 3-D images of hydrogel particles with gold nanocages in D_2O . Since the GNs used in this study were found to have sizes of about 150 nm which are much smaller than the spatial resolution of the NIR multispectral imaging microscope ($0.93 \mu\text{m}/\text{pixel}$), for solutions of (hydrogel particles + GNs), only hydrogel particles were detected and observed by the NIR imaging microscope. As expected, the images of absorption at 1764 nm for three individual hydrogel particles in a solution of (hydrogels+GNs) (Set B, Figure 1) are similar to the image of hydrogel particles without GNs (Set A, Figure 1). It was found, however, that images of hydrogel particles become less focused (or in other words, somewhat defocused) when GNs are added (compare images with (Set B) and without (Set A) GNs). Additionally, it seems that GNs broaden absorption bandwidths of hydrogels (see, for example, the bandwidth of absorption band of a $3.1 \pm 0.4 \mu\text{m}$ hydrogel without GNs in Figure S2B is relatively narrower than spectral bandwidths of three hydrogels with GNs of comparable size ($2.8 \pm 0.3 \mu\text{m}$, $\sim 3.5 \mu\text{m}$) (Figure S3 of Supporting Information)). A variety of reasons might account for these observations, but the most likely one is probably due to the photothermal effect of the GNs. Specifically, it has been reported³² that irradiating nanoparticles may lead to generation of heat and vapor bubbles around the nanoparticles. Because GNs are expected to strongly interact with hydrogel particles, these

effects, in turn, will produce defocusing (of images) and broadening bandwidth of absorption bands of hydrogel particles.³²

The effect of the relative concentration of GNs on the enhancement was subsequently investigated. Three solutions with the same hydrogel concentration but different GN concentrations ($5.6 \times 10^{-12} \text{ M}$ (solution B), $1.4 \times 10^{-11} \text{ M}$ (solution C), and $1.8 \times 10^{-11} \text{ M}$ (solution D)) with solution A, which is without GNs, were prepared, and their multispectral images were recorded. For each solution, at least eight hydrogels particles were measured. 3-D images of some particles for the three solutions with GNs are shown in Figure 2. As illustrated, the enhancement by GNs was found to be strongly dependent on the GN concentration. No enhancement was observed for the lowest concentration of $5.6 \times 10^{-12} \text{ M}$ (Set B in Figure 2 for solution B). Substantial enhancement was observed when the GN concentration was increased to $1.4 \times 10^{-11} \text{ M}$ (Set C for solution C), and $1.8 \times 10^{-11} \text{ M}$ (Set D for solution D). Interestingly, even at higher concentrations, enhancement was not observed for all hydrogel particles. Specifically, out of eight hydrogel particles of solution C, only four particles were found to be enhanced by GNs (image and averaged spectra shown on the right) whereas the remaining four particles were not enhanced, as they have absorption similar to those without GNs (image and averaged spectra shown on the left). Similarly, for solution D, only three out of eight hydrogel particles were found to be enhanced by GNs (images and averaged spectra of enhanced particles on right and unenhanced on left).

Additional information can be obtained by inspecting spectrum of each of eight individual hydrogel particles without GNs and of eight with GNs in four solutions listed above. All 16 spectra for each solution, calculated using data from a single pixel of recorded images, are shown in the first column of Figure S3. They are divided into three sets arranged in three rows for solutions B, C, and D. The first column of each row are spectra of all individual hydrogel particles where those without GNs are shown in blue, and those with GNs are in red. Spectra of each solution were then separated into enhanced spectra (i.e., relatively higher than those for hydrogel without GNs) and unenhanced spectra (i.e., comparable to spectra of hydrogel without GNs). The unenhanced and enhanced spectra were then averaged, and the averaged unenhanced and

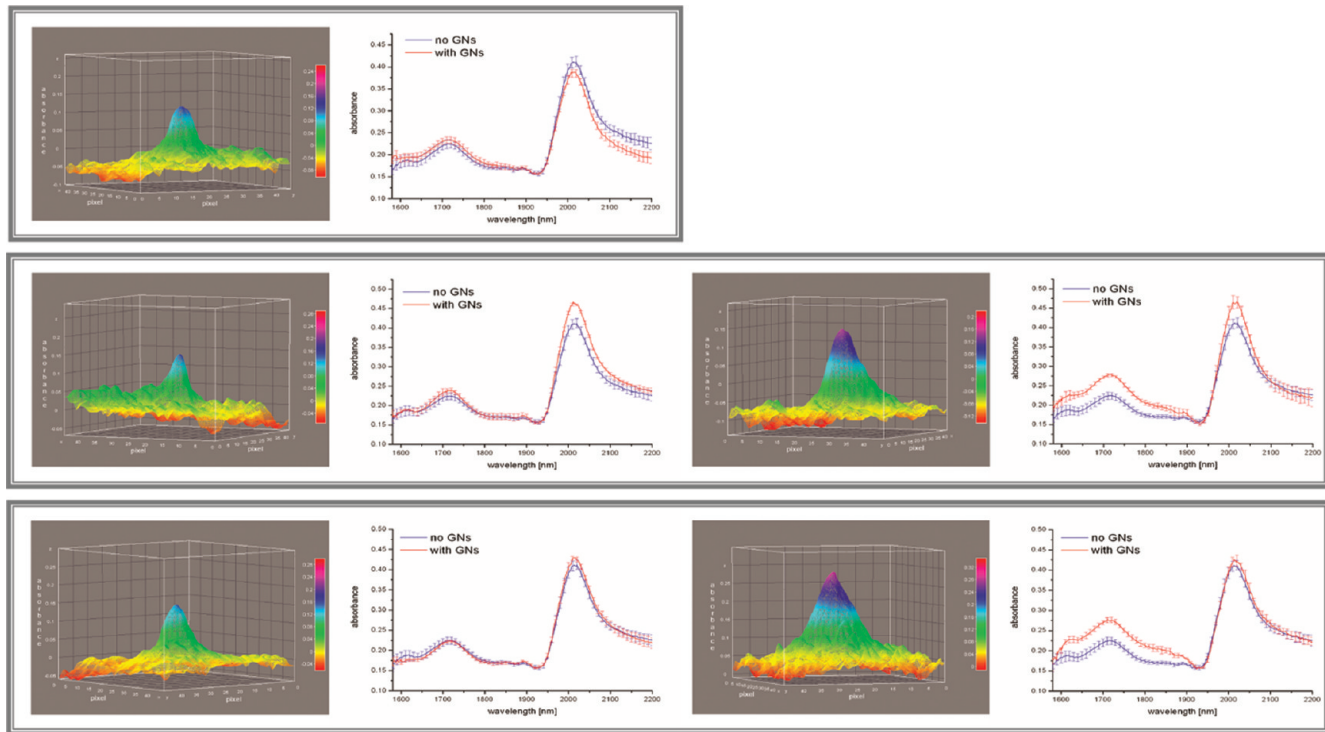


Figure 2. 3-D absorption images of a single hydrogel particle in solutions with different concentrations of GNs: (Set B) with 5.6×10^{-12} M GNs; (Set C) with 1.4×10^{-11} M GNs; (Set D) with 1.8×10^{-11} M GNs. Images in the left column are for unenhanced single hydrogel particles, and images in the right column are for enhanced single hydrogel particles. Spectra (in red) in the left column are average spectra of individual unenhanced hydrogels, and those in the right column are individual enhanced hydrogel particles. For reference, averaged spectra of individual hydrogel particles without GNs are also shown in blue. See text for detailed description.

enhanced spectra for each solution are shown, respectively, in the second and fourth column of Figure 2 (and also in the third and second column of Figure S3).

As can be seen in Figure 2, for solution B, spectra of hydrogels with GNs (in red) are the same, within experimental error, as those without GNs (in blue). This seems to indicate that no enhancement can be observed at a GN concentration of 5.6×10^{-12} M. Increasing the concentration of GNs to 1.4×10^{-11} M (solution C, second row) and 1.8×10^{-11} M (solution D, third row) leads to substantial enhancement in absorption for some. However, as can be seen in the spectra in the second (averaged spectra of unenhanced particles) and fourth columns (averaged spectra of enhanced particles) of both rows, for both solutions, enhancement was found for some but not all hydrogel particles. This is not unexpected, as the concentration of hydrogel particles, which is estimated to be in the 10^{-7} to 10^{-8} M range, is much higher than the concentration of GNs, which is in the 10^{-11} to 10^{-12} M range (see Supporting Information for more information). Since there were not enough GNs to interact with all hydrogel particles in solution, only hydrogel particles which had associated GNs can exhibit enhancement.

While GNs seem to enhance both the 1716 and 2010 nm bands of the hydrogel, the enhancement of the 1716 nm band is more pronounced and has higher reproducibility compared to that for the 2010 nm band. This is possibly because the 1710 nm band is due to C–H groups which are specific to hydrogel particles whereas the 2010 nm band is from O–D groups which are not only in hydrogels but also in D_2O as well.^{33–40}

As detailed in previous studies,^{28,29,33} the size and chemical structure of hydrogels strongly depend on temperature. It is,

therefore, of particular interest to determine if a single hydrogel particle exhibits this behavior as well. Accordingly, we monitored and recorded NIR multispectral images of *a single discrete hydrogel particle* without and with GNs as a function of temperature, by heating the particle solution from room temperature to 57.5 °C and then cooling to 24.0 °C. Shown in Figure 3 are results obtained for hydrogel without (A) and with (B) GNs. Specifically, Set A are 3-D images of an individual hydrogel particle without any GNs, recorded at 1764 nm, during heating process, namely, from room temperature (24.0 °C) to increasing temperatures (25.6 °C, 29.6 °C, 31.3 °C, 34.5 °C, 39.7 °C, 43.7 °C, 46.8 °C, 50.5 °C, and 53.6 °C). The particle solution was then cooled to room temperature (images for cooling period are not shown). As illustrated, the single hydrogel particle can clearly be observed from room temperature up to about 34.5 °C. Thereafter, any additional heating made it increasingly difficult to observe the particle. Interestingly, the particle becomes clearly visible again when it is allowed to cool from 53.6 to 24.0 °C (not shown).

Set B of Figure 3 are images of an individual hydrogel particle with 1.4×10^{-11} M GNs added. These absorption images were recorded at 1764 nm during the same heating process as in the case shown in Set A for the hydrogel without GNs; i.e., from room temperature (23.0 °C) to 25.6 °C, 29.6 °C, 31.3 °C, 34.5 °C, 39.7 °C, 43.7 °C, 46.8 °C, 50.5 °C, and 53.6 °C. It seems that even though temperature has a similar effect on hydrogel particles with GNs as on hydrogels without GNs, the effect is much smaller in the former case. The decrease in absorbance at 1764 nm concomitant with heating the hydrogel particle is

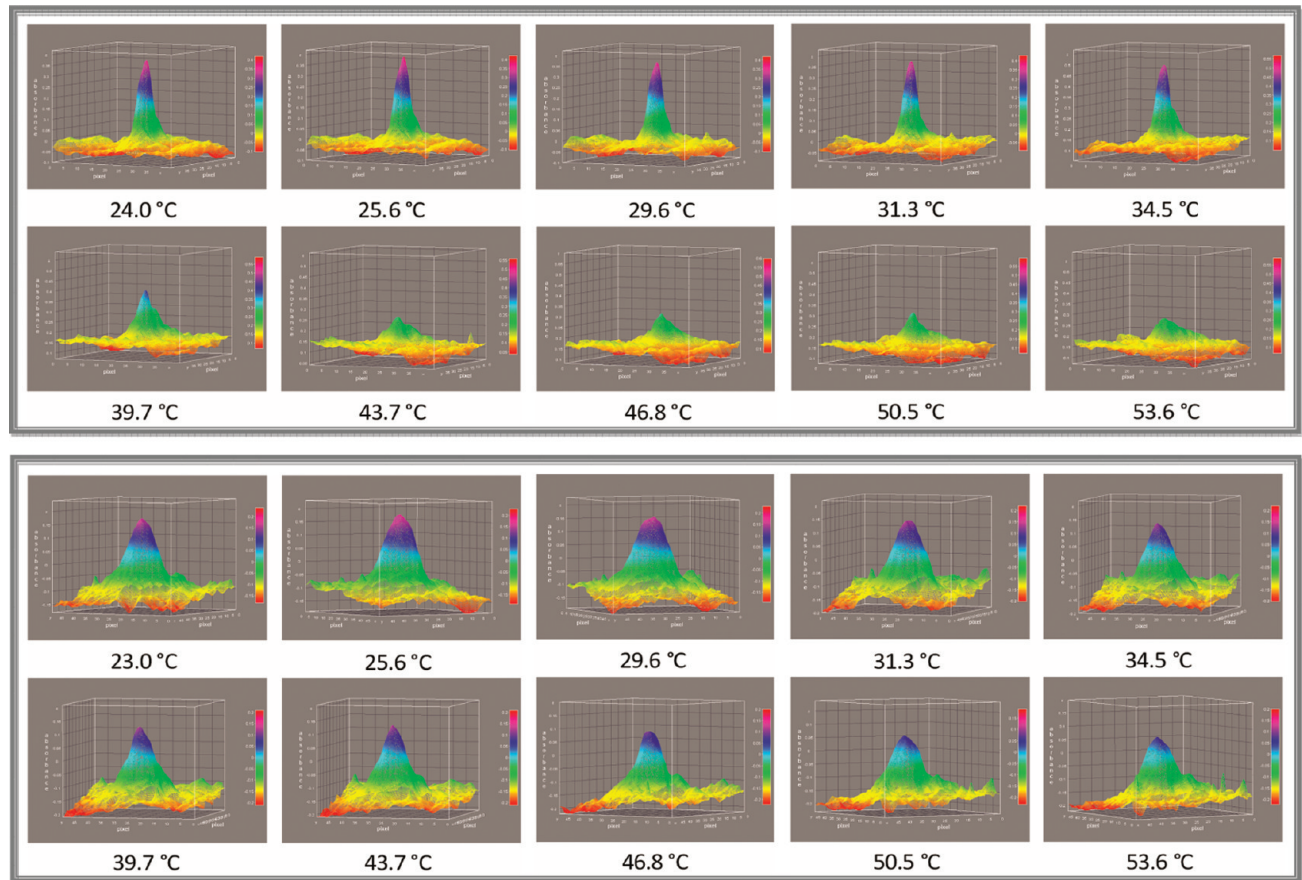


Figure 3. 3-D images of absorption at 1764 nm of the same single hydrogel particle without GNs (Set A) and with 1.4×10^{-11} M GNs (Set B) at 10 different temperatures: from room temperature of 24.0 °C to gradually higher temperatures of 25.6 °C, 29.6 °C, 31.3 °C, 34.5 °C, 39.7 °C, 43.7 °C, 46.8 °C, 50.5 °C, and 53.6 °C. Units for the *x*, *y*, and *z* axes of the 3-D images are pixel, pixel, and absorbance at 1764 nm, respectively, where one pixel corresponds to 0.93 μm .

substantially much smaller when GNs are added. Specifically, in the presence of GNs, and heating to 53.6 °C, absorbance was only decreased by 27.6% which is about 2.5 fold less compared to that in the absence of GNs. More detailed information on the temperature effect on single hydrogel particles without and with GNs can be found in Figures S4 and S5 (of Supporting Information) which show the 2-D and 3-D images during both heating and cooling processes.

As can be seen in the top two sets of spectra shown in the top of Figure 4 (and also in Figure S6 of Supporting Information), additional information on the effect of GNs on the thermal response of hydrogel particles can be obtained by studying the effects of temperature on a single hydrogel particle over the entire NIR spectral region from 1580 and 2200 nm (in contrast to a single wavelength of 1764 nm). Shown in the top of Figure 4 (and also in Figure S6A and S6B) are absorption spectra (which were extracted from recorded images using data from a single pixel) of a single hydrogel particle without (Set A) and with (Set B) added GNs as a function of increasing temperature. Clearly, in both cases, increasing the temperature has a pronounced effect on the spectra of the hydrogel. Specifically, increasing the temperature not only lowers the absorption intensity but also produces a blue shift of the band at ~1716 nm, which arises from C–H overtones and combination transitions.^{30–40} Increasing the temperature also produces a new band at ~1898 nm which has been reported to be due to the hot band of the O–D groups of

the hydrogel particle.^{33,39} It was possible to attribute this hot O–D band not to D₂O but to hydrogel particles because, as explained in details in our previous publication,³³ the same band was observed in spectra when D₂O at the same temperature was used as background (i.e., contribution of D₂O at the same sample temperature was removed from the spectra). While the temperature response of the hydrogel particle is similar in the absence and presence of GNs, the decrease in absorbance of the band at ~1716 nm is much less for the latter compared to the former, namely, the shoulder at ~1620 nm of this band (which can be attributed to CH₂ groups^{33–40}) disappeared when heated for hydrogels without GNs but not for hydrogels with GNs. (This trend can be clearly seen in the bottom figures of Set A and Set B of Supporting Information, which show only 2 of the 14 spectra: spectra at 23.0 °C (black curve) and at 57.5 °C (red curve)). As described above, the fact that enhancement by GNs is higher for the C–H bands compared to that for O–D bands seems to indicate that GNs interact stronger with C–H groups than with the O–D groups, which, as a consequence, may lessen the temperature effect on the C–H bands for hydrogels with GNs.

Additional structural information regarding the hydrogels and their response to temperature can be obtained by carefully inspecting the spectra shown in the top of Set A and Set B (of Figure 4 and Figure S6) for hydrogels without and with GNs, respectively. Shown in the middle row of Figure 4 are plots of the λ_{\max} positions of the 1716 nm band as a function of temperature

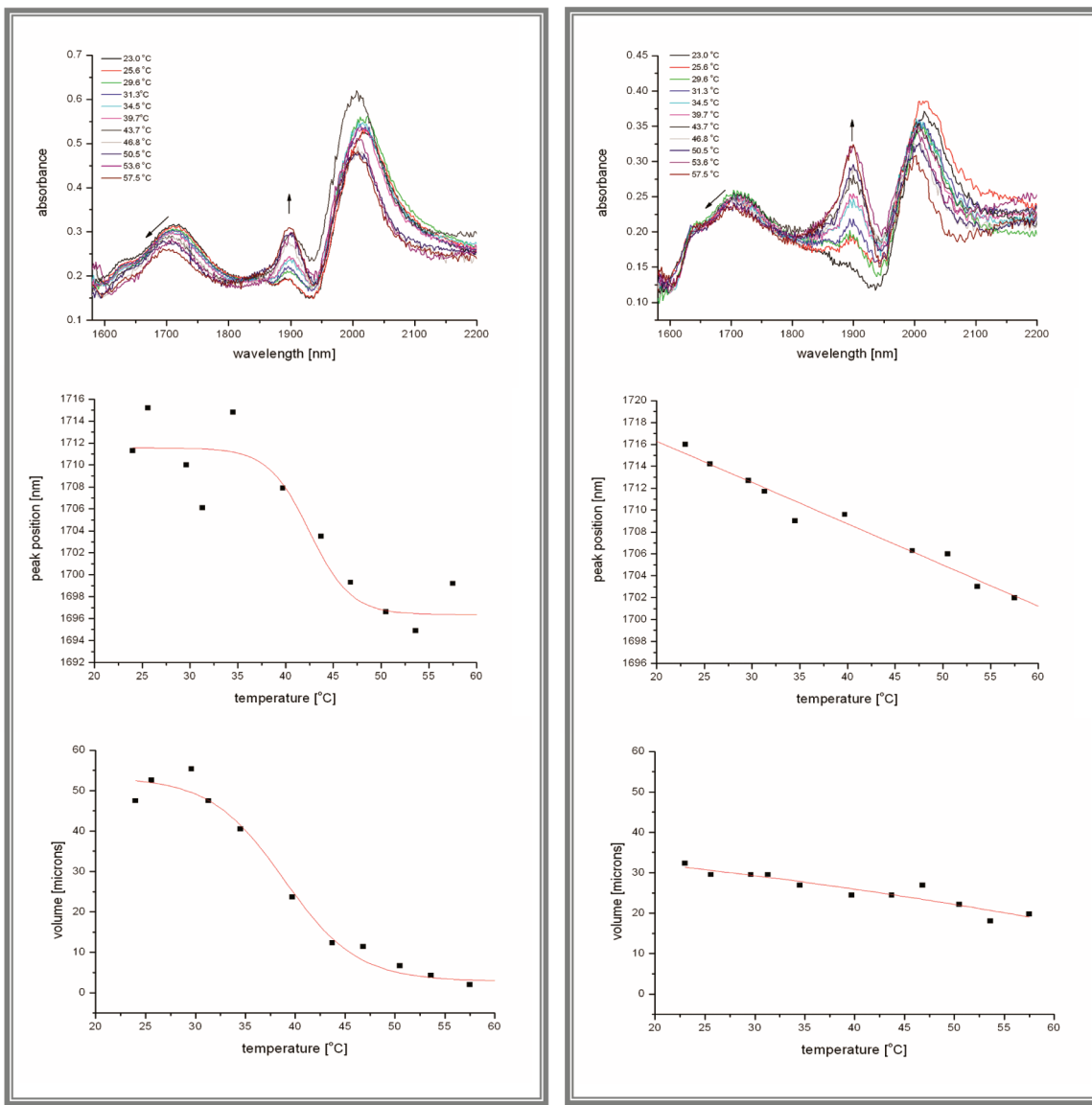


Figure 4. Spectra of a single hydrogel particle in D₂O without GNs are shown in Set A, and spectra with 1.8×10^{-11} M GNs are in Set B. Two sets of spectra shown on the top are absorption spectra of a single hydrogel particle without (A) and with (B) GNs at different temperatures. The middle two curves are plots of λ_{\max} of the C–H band of the same single hydrogel particle without (A) and with (B) GNs as a function of temperature. The change in volume of the same single hydrogel particle without (A low) and with (B low) GNs as a function of temperature is shown in the bottom two curves. See text for detailed description.

for hydrogel without (Set A) and with (Set B) GNs, respectively. It is evident from these plots that for hydrogels without GNs, no significant changes in the λ_{\max} positions occur from room temperature to about 35 °C. However, as the temperature increases further, a substantial decrease in the value of λ_{\max} is observed. Increasing the temperature beyond 45 °C yields a constant λ_{\max} position, which suggests that in the absence of GNs, the hydrogel particle undergoes a phase transition. The phase transition temperature, determined by taking the second derivative of the top curve of Set A, was found to be (42 ± 2 °C). The observed transition of this C–H band might be due, in part, to the fact that upon heating, the hydrogel moieties lose their sphere of hydration, which leads to an increase in the attractive

interactions among the polymer chains (which is reflected by a blue shift of the C–H band). This phenomenon corresponds to the known collapse of the hydrogel network, which leads to a reduction in size.^{7–20} Furthermore, the process is thermally reversible: upon cooling, rehydration of the hydrogel occurs, thereby reverting the particle to its original size (and red-shifting the λ_{\max} to its original position). It is of particular interest to observe in Set B that in the presence of GNs, the hydrogel particle does not exhibit any observable phase transition temperature; rather, the heating of the particle just produced a linear blue shift of the λ_{\max} of the C–H band. The disappearance of the hydrogel phase transition temperature by GNs might be due to the fact described above, namely, irradiating GNs may lead to

generation of heat and vapor bubbles around the GNs. These, in turn, will produce a thermal insulating and defocusing (of images) effect on the hydrogel particles.³²

Rather than indirectly determining the volume transition temperature of individual hydrogel particles from plots of λ_{\max} vs temperature, the volume transition temperature of the hydrogel can be determined directly by plotting hydrogel volume as a function of temperature. This result is possible because each individual hydrogel particle can be observed by the NIR-MSI microscope. Consequently, from the recorded images of the hydrogel particle at different temperatures, the volume of a single hydrogel particle at different temperatures was calculated. The two curves shown in the bottom of Set A and Set B (of Figure 4) are plots of these volumes as a function of temperature for a hydrogel particle without and with GNs, respectively. As illustrated in the bottom curve of Set A, in the absence of GNs, hydrogel particles underwent rapid changes in volume for temperatures from ~ 35 to 45°C . Little or no changes in volume occur above or below this range of temperatures. Phase transition temperature, calculated from the second derivative of the curve shown in the bottom of Figure 4A, was found to be $(39 \pm 4^{\circ}\text{C})$, which agrees well, within experimental error, with the value of $(42 \pm 2^{\circ}\text{C})$ determined by λ_{\max} vs temperature. Again, it is pleasing to see that similar to results obtained with the plot of λ_{\max} vs temperature, in the presence of GNs, heating of hydrogel particles leads not to a transition temperature but rather to a gradual and linear decrease in the particle volume (bottom curve of Set B).

CONCLUSIONS

We have demonstrated that the NIR-MSI microscope can be successfully used to *directly* observe and measure images and spectra of *individual* hydrogel particles alone or with added GNs. Because both images and spectra of the individual particles can be directly and simultaneously measured by the microscope, it is possible to detect any changes in the spectroscopic properties and/or nature (size, volume) of individual hydrogel particles that can be induced by external factors (e.g., temperature and/or pH). These features allow the determination of LCST values based on monitoring either changes in the NIR spectra or the volume of the hydrogel particle in response to variations in temperature. The volume transition temperature or LCST value, *not of a collection of many hydrogel particles, but rather of individual hydrogel particles*, can, therefore, be determined. More importantly, GNs were found to significantly affect not only absorption but also images and properties of individual hydrogel particles. Specifically, GNs were found to enhance absorption of individual hydrogel particles, particularly the C–H band at 1716 nm, by about 25%. Of particular interest is the fact that not all individual hydrogel particles were enhanced by GNs; only about 50% of particles were enhanced by GNs. GNs were also found to cause difficulty for the observation of individual hydrogel particles, i.e., it seems that GNs defocused the images of the hydrogel particles. The defocusing effect by the GNs might be due to photothermal generation of heat and vapor bubbles by the GNs.³² Of particular interest is the effect of GNs on the volume transition temperature of individual hydrogel particles. It seems that individual hydrogel particles lose their LCST in the presence of GNs, i.e., when heated, they undergo a gradual decrease in the volume but do not exhibit any clear and observable discontinued phase transition temperature. Experiments are now in progress to determine the mechanism of the

effects of GNs on absorption, imaging, and volume phase transition of individual hydrogel particles.

ASSOCIATED CONTENT

S Supporting Information. Additional information on instrumentation and performance characteristics of the AOTF-based NIR-MSI microscope, and the synthesis, characterization, and temperature effects on single hydrogel particles without and with GNs, as described in text. This material is available free of charge via the Internet at <http://pubs.acs.org>

AUTHOR INFORMATION

Corresponding Author

*E-mail: chieu.tran@marquette.edu.

ACKNOWLEDGMENT

Acknowledgment is made to Claire Cobley and Younan Xia of Department of Biomedical Engineering, Washington University, St. Louis, for their generous donation of gold nanocages used in this work.

REFERENCES

- Willets, K. A.; Van Duyne, R. P. *Annu. Rev. Phys. Chem.* **2007**, 58, 267–297.
- Skrabalak, S. E.; Chen, J.; Sun, Y.; Lu, X.; Au, L.; Cobley, C. M.; Xia, Y. *Acc. Chem. Res.* **2008**, 41, 1587–1595.
- Sun, Y.; Xia, Y. *Anal. Chem.* **2002**, 74, 5297–5305.
- Song, K. H.; Kim, C.; Cobley, C. M.; Xia, Y.; Wang, L. V. *Nano Lett.* **2009**, 9, 183–188.
- Chen, J.; Saeki, F.; Wiley, B. J.; Cang, H.; Cobb, M. J.; Li, Z.-Y.; Au, L.; Zhang, H.; Kimmey, M. B.; Li, X.; Xia, Y. *Nano Lett.* **2005**, 5, 473–477.
- Yavuz, M. S.; Cheng, Y.; Chen, J.; Cobley, C. M.; Zhang, Q.; Rycenga, M.; Xie, J.; Kim, C.; Song, K. H.; Schwartz, A. G.; Wang, L. V.; Xia, Y. *Nat. Mater.* **2009**, 8, 1–5.
- Peppas, N. A.; Huang, Y.; Torres-Lugo, M.; Ward, J. H.; Zhang, J. *Annu. Rev. Biomed. Eng.* **2000**, 2, 9–29.
- Hirotsu, S.; Hirokawa, Y.; Tanaka, T. *J. Chem. Phys.* **1987**, 87, 1392–1395.
- Hirokawa, Y.; Tanaka, T. *J. Chem. Phys.* **1984**, 81, 6379–6380.
- Li, Y.; Tanaka, T. *Annu. Rev. Mater. Sci.* **1992**, 22, 243–277.
- Bromberg, L.; Temchenko, M.; Alakhov, V.; Hatton, T. A. *Langmuir* **2005**, 21, 1590–1598.
- Beebe, D. J.; Moore, J. S.; Bauer, J. M.; Yu, Q.; Liu, R. H.; Devadoss, C.; Jo, B.-H. *Nature* **2000**, 404, 588–590.
- Kawasaki, H.; Sasaki, S.; Maeda, H. *Langmuir* **1998**, 14, 773–776.
- Shibayama, M.; Mizutani, S.; Nomura, S. *Macromolecules* **1996**, 29, 2019–2025.
- Zhou, S.; Chu, B. *J. Phys. Chem. B* **1998**, 102, 1364–1368.
- Snowden, M. J.; Chowdhry, B. Z.; Vincent, B.; Morris, G. E. *J. Chem. Soc., Faraday Trans.* **1996**, 92, 5013–5016.
- Lamanna, R.; Sobolev, A. P.; Masci, G.; Bontempo, D.; Crescenzi, V.; Segre, A. L. *Polym. Prepr.* **2003**, 44, 406–407.
- Datta, A.; Das, S.; Mandal, D.; Pal, S.; Bhattacharyya, K. *Langmuir* **1997**, 13, 6922–6926.
- Iwai, K.; Hanasaki, K.; Yamamoto, M. *J. Lumin.* **2000**, 87–89, 1289–1291.
- Masci, G.; Cametti, C. *J. Phys. Chem. B* **2009**, 113, 11421–11428.
- Tran, C. D.; Cui, Y.; Smirnov, S. *Anal. Chem.* **1998**, 70, 4701–4708.
- Fischer, M.; Tran, C. D. *Anal. Chem.* **1999**, 71, 953–959.

- (23) Fischer, M.; Tran, C. D. *Anal. Chem.* **1999**, *71*, 2255–2261.
- (24) Khait, O.; Smirnov, S.; Tran, C. D. *Anal. Chem.* **2001**, *73*, 732–739.
- (25) Tran, C. D.; Grishko, V. I.; Challa, S. *J. Phys. Chem. B* **2008**, *112*, 14548–14559.
- (26) Mejac, I.; Bryan, W. W.; Lee, T. R.; Tran, C. D. *Anal. Chem.* **2009**, *81*, 6687–6694.
- (27) Morris, M. D. *Microscopic and Spectroscopic Imaging of the Chemical State*; Marcel Dekker: New York, 1993.
- (28) Debord, S. B.; Lyon, L. A. *J. Phys. Chem. B* **2003**, *107*, 2927–2932.
- (29) Tagit, O.; Tomczak, N.; Vancso, G. J. *Small* **2008**, *4*, 119–126.
- (30) Im, S. H.; Lee, Y. T.; Wiley, B.; Xia, Y. *Angew. Chem., Int. Ed.* **2005**, *44*, 2154–2157.
- (31) Skrabalak, S. E.; Au, L.; Li, X.; Xia, Y. *Nature Protoc.* **2007**, *2*, 2182–2190.
- (32) Lapotko, D. *Fut. Med.* **2009**, *4*, 813–845.
- (33) Mejac, I.; Park, H. H.; Bryan, W. W.; Lee, T. R.; Tran, C. D. *Anal. Chem.* **2010**, *82*, 1698–1704.
- (34) Schmidt, P.; Dybal, J.; Trchova, M. *Vib. Spectrosc.* **2006**, *42*, 278–283.
- (35) Sun, B.; Lin, Y.; Wu, P.; Siesler, H. W. *Macromolecules* **2008**, *41*, 1512–1520.
- (36) Czarmecki, M. A.; Haufa, K. Z. *J. Phys. Chem. A* **2005**, *109*, 1015–1021.
- (37) Langford, V. S.; McKinley, A. J.; Quackenden, T. I. *J. Phys. Chem. A* **2001**, *105*, 8916–8921.
- (38) Waggener, W. C. *Anal. Chem.* **1956**, *30*, 1569–1570.
- (39) Harvey, D. K.; Feierabend, K. J.; Black, J. C.; Vaida, V. *J. Mol. Spectrosc.* **2005**, *229*, 151–157.
- (40) Geuken, B.; Meersman, F.; Nies, E. *J. Phys. Chem. B* **2008**, *112*, 4474–4477.